The transcriptional landscape of the developing chick trigeminal ganglion

Carrie E. Leonard[1], Alec McIntosh[2], Lisa A. Taneyhill[1,*]

[1]Department of Animal and Avian Sciences, University of Maryland, College Park, MD 20742 USA

[2]Lombardi Comprehensive Cancer Center, Georgetown University, Washington, DC, 20007 USA

*Corresponding author; Email: ltaney@umd.edu

Keywords: Trigeminal ganglion, neural crest cells, placode cells, RNA-sequencing

Funding information: NIH R01DE024217

Summary

The trigeminal ganglion is a critical structure in the peripheral nervous system, responsible for transmitting sensations of touch, pain, and temperature from craniofacial regions to the brain. Trigeminal ganglion development depends upon intrinsic cellular programming as well as extrinsic signals exchanged by diverse cell populations. With its complex anatomy and dual cellular origin from cranial placodes and neural crest cells, the trigeminal ganglion offers a rich context for examining diverse biological processes, including cell migration, fate determination, adhesion, and axon guidance. Avian models have, so far, enabled key insights into craniofacial and peripheral nervous system development. Yet, the molecular mechanisms driving trigeminal ganglion formation and subsequent nerve growth remain elusive. In this study, we performed RNA-sequencing at multiple stages of chick trigeminal ganglion development and generated a novel transcriptomic dataset that has been curated to illustrate temporally dynamic gene expression patterns. This publicly available resource identifies major pathways involved in trigeminal gangliogenesis, particularly with respect to the condensation and maturation of placode-derived neurons, thus inviting new lines of research into the essential processes governing trigeminal ganglion development.

Introduction

The trigeminal ganglion is responsible for relaying sensations like touch, pain, and temperature from the face and oral cavity to the central nervous system[1]. Trigeminal dysfunction causes disabling conditions including migraine headache, orofacial pain, and chronic dry eye, whose etiologies remain poorly understood[2–4]. Hereditary disorders associated with cranial sensory deficits are also explained, in part, by altered trigeminal nerve development[5–7]. Despite clear relevance to human health, the genetic landscape and molecular mechanisms underlying trigeminal ganglion neurodevelopment are still poorly characterized.

Peripheral nervous system development begins early during embryogenesis, at stages that are difficult to access in mammals. Avian studies have historically offered critical insight into the cellular lineage and molecular processes that govern cranial gangliogenesis[8–10]. Primary sensory neurons reside in peripheral sensory ganglia which are largely derived from the neural crest, a transient, multipotent progenitor population that gives rise to diverse tissues during vertebrate embryogenesis[11]. Likewise, cranial ganglia contain neural crest-derived sensory neurons and glia while also receiving neuronal contributions from specialized ectodermal

thickenings called placodes[12]. While most cranial ganglia contain either neural crest- or placode-derived neurons that are spatially distinct, the trigeminal ganglion uniquely comprises a mixed neuronal population arising from both lineages[13,14]. Development of a functional trigeminal ganglion relies upon intrinsic transcriptional programming as well as reciprocal communication between neural crest and placode cells[15–18].

Cranial neural crest cells, which originate in the dorsal neural folds and migrate to their final destinations within the embryo, influence the differentiation, migration, and growth of placode cells[19–21]. Chemotactic cues are sent by both neural crest and placode cells to direct their migration to the trigeminal ganglion anlage[22,23]. In tandem, migratory neural crest cells create corridors through which placodal neurons travel after delaminating from the overlying ectoderm[24,25]. Neurogenesis is staggered between the two progenitor populations, such that placode cells are the first to adopt a neuronal fate, followed by neural crest cells, which will also give rise to glia[26,27]. The coalescence and condensation of placodal neurons with undifferentiated neural crest cells to form the ganglion is mediated by cell adhesion molecules including Cadherins[28,29], and signaling pathways, like Wnt and Slit/Robo[29–31]. Once the earliest trigeminal sensory axons extend from placodal neurons, their growth toward craniofacial sites of innervation is further guided by diffusible factors, such as BMPs[32], semaphorins[33,34], and neurotrophins[35,36]. Thus, the developing trigeminal ganglion and its required interactions between neural crest cells and placodal neurons offer a rich context in which to investigate core biological processes, from fate determination to cell migration to axon guidance.

From decades of elegant work conducted in vertebrate embryos, there is a strong foundational understanding of neural crest and placode cell interactions and their contributions to cranial ganglia[37,38]. However, studies characterizing neurodevelopment from placodes are underrepresented compared to our knowledge of neural crest-derived neurons[39]. The early development and lack of genetic tools to target specific placodal subpopulations in mammalian models hinders research progress in this area. In contrast, chick embryos offer relative ease of access to facilitate the experimental manipulation of neural crest and distinct placodal progenitors[40], with the additional benefit of continued development *in ovo*. With the evolutionary conservation of developmental mechanisms between species[38,41,42], the chick embryo remains a favored, economical model for examining embryonic development, including neurogenic cranial placodes.

To elucidate normal gene expression dynamics during trigeminal ganglion development, we performed RNA-sequencing at sequential timepoints and curated a novel transcriptomic dataset to illustrate relative changes in gene expression over time. Data are shared in the FaceBase repository (NIDCR, Accession # pending) to encourage further exploration by researchers interested in craniofacial and/or peripheral nervous system development. Our findings identify key pathways involved in trigeminal gangliogenesis and provide critical insight into the molecular mechanisms underlying neurodevelopment and cellular interactions between placode-derived neurons and neural crest cells.

Methods

Collection of trigeminal ganglia from chick embryos

Fertilized chicken eggs (*Gallus gallus*) were procured from Hy-Line North America (Elizabethtown, PA) or Centurion Poultry (Lexington, GA) and incubated in a humid environment at 37 degrees Celsius. Embryos were staged using the Hamburger-Hamilton (HH) method[43], then removed from the egg and placed into sterile, ice-cold Ringer's solution (0.125M sodium chloride, 1.5mM calcium chloride dihydrate, 5mM potassium chloride, 0.8mM sodium phosphate dibasic, adjusted to pH 7.4). Trigeminal ganglia were dissected using electrolytically sharpened tungsten needles, pooled by appropriate stages, and flash frozen in liquid nitrogen until total RNA extraction. With three pooled biological replicates for each stage, a total of 47 ganglia were used from HH13/14 embryos, 47 ganglia from HH15/16 embryos, and 56 ganglia from HH17/18 embryos.

RNA extraction, library preparation, RNA-sequencing and data processing

Total RNA was isolated according to the manufacturer's protocol for the RNAqueous Total RNA Isolation kit (ThermoFisher, #AM1912). RNA concentration and integrity were quantified with Nanodrop (ThermoFisher) and Agilent 2100 bioanalyzer. The TruSeq sample preparation kit (Illumina) was used to generate poly(A)-enriched cDNA libraries, followed by assessment of quality and quantity using the bioanalyzer. 100bp paired-end reads were obtained with the Illumina HiSeq 1500 platform. Illumina adapter sequences were removed using Trimmomatic[44] and the quality of reads assessed with FastQC[45]. HISAT2[46] was used to align reads with a *Gallus gallus* reference genome (bGalGal1.mat.broiler.GRCg7b) and the number of reads per gene was quantified using HTSeq[47]. Differential expression analyses were performed on normalized counts using DESeq2[48], with three biological replicates from pooled trigeminal ganglia per indicated stage bin, and two technical replicates per biological replicate

included. Raw sequencing data is publicly available in the FaceBase repository at https://www.facebase.org (NIDCR, Accession # pending). Text files with normalized gene counts and DESeq2-identified differentially expressed genes are attached as supplemental files.

Polar Plot and Gene Ontology Enrichment Analyses

Normalized differential expression data were first used to calculate "H" by transforming sequential data (T^0-T^1-T^2) into angular values representing relative gene expression at HH13/14 (T^0), HH15/16 (T^1), and HH17/18 (T^2), respectively[49,50]. The determined angular values illustrate expression dynamics (i.e., low-low-high) on a radial plot. "H" corresponds to the relative angular position of individual gene expression across T^0-T^1-T^2 (i.e., yellow; H=0 degrees indicates no change from T^0-T^1, and a significant increase in gene expression from T^1-T^2). MaxLog, as determined with DESeq2 as the maximal Log_2 fold change between any two timepoints, is illustrated in the polar plot as distance from the center, while the transparency of a particular point reflects the average normalized gene expression of a given gene (i.e., values greater than 100 are fully opaque whereas lower averages are more transparent). Polar plots were generated with *ggplot2*[51] and scaled expression profiles were created in R using previously described equations[52] adapted from the Mandrup group[49,50]. Briefly, relative mean changes in gene expression were transformed to an angle between -180 and +180 degrees, then further transformed to a scale from 0 to 360 degrees, which was used to determine color based on degree. Differentially expressed genes were plotted using polar coordinates with the radius equal to MaxLog, and angular position around the radial plot determined by the change trend. Color-coded, three-point profile annotations demonstrating relative expression changes corresponding from left to right as HH13/14 (T^0), HH15/16 (T^1), and HH17/18 (T^2), respectively, are displayed every 30 degrees along the outer edge of the polar plot. For Gene Ontology enrichment, genes were parsed into six sectors by grouping profiles into 60-degree intervals starting at 0 degrees, which denotes genes that were unchanged between T^0-T^1, but significantly increased from T^1-T^2. Using *EnrichR*[53–55], genes within each 60-degree sector were assessed against the GO Biological Process and GO Cellular Compartment databases[56]. Prism (Graphpad) was used to graph the top fifteen pathways most enriched for each sector based on p-value. Excel files summarizing all color-matched calculated values for the polar plot and sector-parsed GO analyses are attached as supplemental files.

Results and Discussion

To elucidate gene expression dynamics and identify key molecular drivers of trigeminal ganglion development, we performed a bulk RNA-sequencing time course assay. Trigeminal ganglia were collected from chicken embryos, pooled into three Hamburger-Hamilton (HH) stage-dependent bins[43] (HH13/14, HH15/16, or HH17/18), and separated into three biological replicates per bin before RNA extraction. A total of 47 trigeminal ganglia were used from HH13/14 embryos, corresponding to a time when placodal neurons and neural crest cells begin to coalesce within the trigeminal ganglion anlage. HH15/16 trigeminal ganglia (n=47) are in the process of condensing into a compact structure, comprising a mixture of neural crest cells and placodal neurons that have initiated neurite extension. By HH17/18 (n=56), the trigeminal ganglion is densely populated with placodal neurons that are actively undergoing axon growth and guidance, comingled with neural crest cells that have not yet differentiated into neurons or glia. Our goal was not only to detect differentially expressed genes, but to visualize the dynamic patterns spanning these three developmental timepoints. To this end, polar plots were created to summarize the relative relationships of individual genes from HH13/14 to HH15/16 to HH17/18, and cluster genes into groups based on similar temporal dynamics (Figure 1)[49,50].

In total, 14,506 genes were detected across the three timepoints. 5,703 genes exhibited significant differential expression ($p<0.05$ after Benjamini-Hochberg correction, see Supplemental File 1) at one timepoint compared to at least one other and were included in the polar plot (Figure 1A) and associated histogram (Figure 1B). The upregulation or downregulation of individual differentially expressed genes from HH13/14 to HH15/16 to HH17/18 was transformed into angular representations of relative expression over time, and placed onto a circular spectrum, where position around the circle is analogous to angular expression profiles, which are color-coded based on the degree within the circle, i.e., 0 degrees (yellow) is analogous to no change between HH13/14 and HH15/16, then a significant increase from HH15/16 to HH17/18 (Figure 1A). Of the differentially expressed genes, there were 765 with a maximal Log_2 fold change (MaxLog) greater than 1.0, 124 genes with MaxLog greater than 2.0, and 14 genes with MaxLog exceeding 4.0 in any comparison, as indicated by increasing distance from the center of the polar plot (Figure 1A). Generally, the greatest changes in expression occurred in those genes exhibiting a temporal profile with upregulation between HH13/14 and HH15/16 (green to blue on polar plot), and either upregulation (yellow to green on polar plot) or sustained expression (green to blue on polar blot) from HH15/16 to HH17/18 (Figure 1A). The greatest numbers of differentially expressed genes occurred between

0 and +60 degrees (yellow to green) and between -120 and -180 degrees (indigo to purple) on the polar plot (Figure 1B), suggesting most changes in gene expression are unidirectional and/or sustained over time, regardless of increased versus decreased expression.

To understand how shared temporal gene expression profiles relate to biological events occurring in the developing trigeminal ganglion from HH13/14 to HH17/18, and to identify which genes may play a role in these processes, the polar plot was divided into 60-degree sectors. Differentially expressed genes within any given 60-degree sector displayed similar expression trajectories, on average, and were assessed for Gene Ontology (GO) enrichment against the GO: Biological Processes and GO: Cellular Component databases[56] (Figures 2-3, Supplemental Figures 1-4, Supplemental File 2).

Within Sector 1, 1900 genes exhibited expression profiles that, on average, increased consistently from HH13/14 to HH15/16 and from HH15/16 to HH17/18, with some variation at the mid-point, but consistent upregulation by HH17/18 when compared to HH13/14 (Figure 2A and 2B). Significant biological processes and components associated with Sector 1 genes included Axonogenesis, Axon Guidance, Positive Regulation of Neuron Projection Development, Neuron Projection, Axon, and Cytoskeleton (Figure 2C and 2D). These findings align with the ongoing arrival and maturation of placodal neurons in the trigeminal ganglion between HH13/14 and HH17/18. While key signaling pathways known to be involved in sensory axon growth and guidance were among the upregulated genes in Sector 1, including Eph receptors, Semaphorins, and Notch (Figure 2C, right panel), genes within these families have not been well characterized in the trigeminal ganglion. Additionally, the GO enrichment results indicated changes in cell migration, cell signaling, and interactions with the extracellular matrix (Figure 2C and 2D). Such molecular changes may act to slow the migration of placodal neurons and/or neural crest cells as they populate the trigeminal ganglion and mature over time. They may also reflect genes important for sensing the environment as axons grow in search of their respective target tissues, or as neural crest cells process extracellular cues that trigger differentiation.

In Sector 2, 796 genes, on average, were upregulated at HH15/16 compared to HH13/14, with sustained, but not further increased, expression at HH17/18 (Figure 3A and 3B). Differential expression of Sector 2 genes reflected activation of pathways involved in autophagy, as evidenced by enrichment in categories including Lysosomal Transport, Positive Regulation of Autophagy, Vesicle-Mediated Transport, Lysosome, Recycling Endosome, and Autophagosome (Figure 3C and 3D). While autophagy is a key player in processes including migration and differentiation that could be occurring in multiple cell types, it is also essential for proper

neuronal development, plasticity, and survival[57,58]. Indeed, several neurodevelopmental disorders associated with sensory deficits, including autism spectrum disorders, are linked to dysfunctional autophagy[59]. Little has been described regarding the role of autophagy in trigeminal ganglion neurodevelopment, yet our findings indicate a large proportion of differentially expressed genes may participate in this process as placodal neurons mature. While genes identified in Sectors 1 and 2 are largely associated with neurodevelopmental mechanisms, it is also plausible that they are driven by transcriptional changes in neural crest cells or even cranial mesenchyme, as multiple populations are present in our samples. Follow-up studies are needed to determine the unique cellular localization of differentially expressed transcripts, and how the identified pathways may function in placodal neurons versus neural crest cells at the examined timepoints.

Overall, genes in Sector 3 were associated with temporary upregulation of processes including sensory perception, glucose and ion transport, homeostasis, and cytoskeletal reorganization at HH15/16 (Supplemental Figure 1). Such processes are important for cell-cell communication, which is critical as undifferentiated neural crest cells and placodal neurons further condense to generate the ganglion, including supporting morphological changes in both cell populations[60–62]. Downregulated genes in Sectors 4 and 5 that remained lower at HH17/18 were generally associated with negative regulation of gene expression and protein biogenesis (Supplemental Figures 2-3). These findings may mirror trigeminal ganglion cells as they transition from proliferative and/or migratory progenitor states into cells with more defined fates, such as the increasing number of post-mitotic placodal neurons in the trigeminal ganglion over time, or neural crest cells that are poised to differentiate into glia and neurons. Finally, the expression profiles of genes in Sector 6 generally reflected a temporary decrease in mitochondrial metabolic processes and cell motility (Supplemental Figure 4). This pattern may, too, reflect a pause and restructuring of energy-dependent cellular processes needed to support later steps in gangliogenesis, including axon extension and transport for neurodevelopment[63,64]. These non-exhaustive hypotheses require further investigation in order to fully understand the implications of individual gene expression trends in specific cell types.

Interpretation of our data is limited by the inability to assign changes in individual gene expression to a particular cell population. The RNA-sequencing data was generated from whole trigeminal ganglion lysate and, therefore, encompasses both placodal neurons and neural crest cells that are present in staggered stages of development. Moreover, tissue samples likely included some contamination from the surrounding mesenchyme, especially at stages that

precede trigeminal ganglion condensation. Given the migratory nature of several cell populations during the examined stages of craniofacial development, it is also possible that some transient changes in gene expression (for example, genes in Sectors 3 or 6) are explained by cells in transit to other tissues that do not ultimately remain in the trigeminal ganglion. Advantageously, our data more broadly captures genes that are dynamically expressed in newly differentiated, immature placodal neurons compared to previously published work that excluded younger neurons from analysis[65]. In both cases, however, RNA-sequencing, while informative, does not account for post-transcriptional or post-translational mechanisms that control gene expression. Follow-up assessment of protein products compared to their respective transcript profiles would provide additional insight into the functional consequences of the described transcriptional dynamics.

Conclusions

Our report visually and quantitatively illustrates temporal dynamics in gene expression, cellular events, and key molecular pathways that participate in the development of the trigeminal ganglion in chick. These gene signatures correspond to key stages in trigeminal gangliogenesis, from the time when neural crest and placode cells coalesce and form a cohesive structure, through the neuronal maturation and early axon extension of placodal neurons. This novel, publicly available dataset is processed and curated with the goal of inspiring new lines of investigation into the molecular mechanisms underlying cranial sensory neuron development and the cellular interactions required for proper craniofacial development during embryogenesis.

Acknowledgements

We thank Chyong-Yi Wu, Ph.D. for technical assistance in sample preparation. We thank Sue Zhao, Ph.D, Hector Corrada Bravo, Ph.D., and the UMD Institute for Bioscience & Biotechnology Research for their technical assistance and expertise in sequencing and preliminary data analyses.

References

1. Sanders, R. D. The Trigeminal (V) and Facial (VII) Cranial Nerves: Head and Face Sensation and Movement. *Psychiatry (Edgmont)* **7**, 13–6 (2010).

2. Olesen, J., Burstein, R., Ashina, M. & Tfelt-Hansen, P. Origin of pain in migraine: evidence for peripheral sensitisation. *The Lancet Neurology* vol. 8 679–690 Preprint at https://doi.org/10.1016/S1474-4422(09)70090-0 (2009).

3. Soares, F. *et al.* Effect of Genetic Polymorphisms on Pain Sensitivity in the Orofacial Region: A Systematic Review. *J Oral Facial Pain Headache* **34**, 353–363 (2020).

4. Patel, S., Hwang, J., Mehra, D. & Galor, A. Corneal Nerve Abnormalities in Ocular and Systemic Diseases. *Exp Eye Res* **202**, 108284 (2021).

5. Leonard, C. E., Quiros, J., Lefcort, F. & Taneyhill, L. A. Loss of Elp1 disrupts trigeminal ganglion neurodevelopment in a model of familial dysautonomia. *Elife* **11**, (2022).

6. Karpinski, B. A. *et al*. Selective disruption of trigeminal sensory neurogenesis and differentiation in a mouse model of 22q11.2 deletion syndrome. *DMM Disease Models and Mechanisms* **15**, (2022).

7. Schwartzlow, C. & Kazamel, M. Hereditary Sensory and Autonomic Neuropathies: Adding More to the Classification. *Curr Neurol Neurosci Rep* **19**, (2019).

8. Le Douarin, N. M. The avian embryo as a model to study the development of the neural crest: A long and still ongoing story. *Mechanisms of Development* vol. 121 1089–1102 Preprint at https://doi.org/10.1016/j.mod.2004.06.003 (2004).

9. Hamburger, V. Experimental analysis of the dual origin of the trigeminal ganglion in the chick embryo. *Journal of Experimental Zoology* **148**, 91–123 (1961).

10. Méndez-Maldonado, K., Vega-López, G. A., Aybar, M. J. & Velasco, I. Neurogenesis From Neural Crest Cells: Molecular Mechanisms in the Formation of Cranial Nerves and Ganglia. *Frontiers in Cell and Developmental Biology* vol. 8 Preprint at https://doi.org/10.3389/fcell.2020.00635 (2020).

11. Bronner, M. E. & LeDouarin, N. M. Development and evolution of the neural crest: An overview. *Developmental Biology* vol. 366 2–9 Preprint at https://doi.org/10.1016/j.ydbio.2011.12.042 (2012).

12. D'Amico-Martel, A. & Noden, D. M. Contributions of placodal and neural crest cells to avian cranial peripheral ganglia. *Am J Anat* **166**, 445–468 (1983).

13. Lwigale, P. Y. Embryonic origin of avian corneal sensory nerves. *Dev Biol* **239**, 323–337 (2001).

14. Hamburger, V. Experimental analysis of the dual origin of the trigeminal ganglion in the chick embryo. *Journal of Experimental Zoology* **148**, 91–123 (1961).

15. Moody, S. A. & LaMantia, A.-S. Transcriptional Regulation of Cranial Sensory Placode Development. in *Curr Top Dev Biol* vol. 111 301–350 (2015).

313 16. Wu, C. Y. & Taneyhill, L. A. Cadherin-7 mediates proper neural crest cell–placodal neuron
314 interactions during trigeminal ganglion assembly. *Genesis* **57**, 1–14 (2019).

315 17. Wu, C. Y., Hooper, R. M., Han, K. & Taneyhill, L. A. Migratory neural crest cell αN-catenin impacts
316 chick trigeminal ganglia formation. *Dev Biol* **392**, 295–307 (2014).

317 18. Halmi, C. A., Wu, C. Y. & Taneyhill, L. A. Neural crest cell-placodal neuron interactions are
318 mediated by Cadherin-7 and N-cadherin during early chick trigeminal ganglion assembly.
319 *F1000Res* **11**, 741 (2022).

320 19. Steventon, B., Mayor, R. & Streit, A. Neural crest and placode interaction during the development
321 of the cranial sensory system. *Dev Biol* **389**, 28–38 (2014).

322 20. Theveneau, E. & Mayor, R. Neural crest delamination and migration: From epithelium-to-
323 mesenchyme transition to collective cell migration. *Developmental Biology* vol. 366 34–54
324 Preprint at https://doi.org/10.1016/j.ydbio.2011.12.041 (2012).

325 21. Leonard, C. E. & Taneyhill, L. A. The road best traveled: Neural crest migration upon the
326 extracellular matrix. *Seminars in Cell and Developmental Biology* vol. 100 177–185 Preprint at
327 https://doi.org/10.1016/j.semcdb.2019.10.013 (2020).

328 22. Gammill, L. S., Gonzalez, C., Gu, C. & Bronner-Fraser, M. Guidance of trunk neural crest migration
329 reguires neuropilin 2/semaphorin 3F signaling. *Development* **133**, 99–106 (2006).

330 23. Guidato, S. & Itasaki, N. Wise retained in the endoplasmic reticulum inhibits Wnt signaling by
331 reducing cell surface LRP6. *Dev Biol* **310**, 250–263 (2007).

332 24. Freter, S., Fleenor, S. J., Freter, R., Liu, K. J. & Begbie, J. Cranial neural crest cells form corridors
333 prefiguring sensory neuroblast migration. *Development (Cambridge)* **140**, 3595–3600 (2013).

334 25. Barlow, L. A. *Cranial Nerve Development: Placodal Neurons Ride the Crest*. *Current Biology* vol. 12
335 (2002).

336 26. Noden', D. M. *An Analysis of the Migratory Behavior of Avian Cephalic Neural Crest Cells'*.
337 *DEVELOPMENTAL BIOLOGY* vol. 42 (1975).

338 27. D'amico-Martel, A. & Noden, D. An autoradiographic analysis of the development of the chick
339 trigeminal ganglion. *J Embryol Exp Morphol* **55**, 167–182 (1980).

340 28. Wu, C. Y. & Taneyhill, L. A. Cadherin-7 mediates proper neural crest cell–placodal neuron
341 interactions during trigeminal ganglion assembly. *Genesis* **57**, 1–14 (2019).

342 29. Shiau, C. E. & Bronner-Fraser, M. N-cadherin acts in concert with Slit1-Robo2 signaling in
343 regulating aggregation of placode-derived cranial sensory neurons. *Development* **136**, 4155–4164
344 (2009).

345 30. Shiau, C. E., Lwigale, P. Y., Das, R. M., Wilson, S. A. & Bronner-Fraser, M. Robo2-Slit1 dependent
346 cell-cell interactions mediate assembly of the trigeminal ganglion. *NATURE NEUROSCIENCE*
347 *VOLUME* **11**, (2008).

348 31. Shigetani, Y. *et al.* Wise promotes coalescence of cells of neural crest and placode origins in the
349 trigeminal region during head development. *Dev Biol* **319**, 346–358 (2008).

350 32. Hodge, L. K. *et al.* Retrograde BMP Signaling Regulates Trigeminal Sensory Neuron Identities and
351 the Formation of Precise Face Maps. *Neuron* **55**, 572–586 (2007).

352 33. William Rochlin, M. & Farbman, A. I. *Trigeminal Ganglion Axons Are Repelled By Their*
353 *Presumptive Targets*. (1997).

354 34. Chen, H. *et al.* Neuropilin-2 Regulates the Development of Select Cranial and Sensory Nerves and
355 Hippocampal Mossy Fiber Projections. *Neuron* **25**, 43–56 (2000).

356 35. O'Connor, R. & Tessier-Lavigne, M. Identification of Maxillary Factor, a Maxillary Process–Derived
357 Chemoattractant for Developing Trigeminal Sensory Axons. *Neuron* **24**, 165–178 (1999).

358 36. Enokido, Y., Wyatt, S. & Davies, A. M. Developmental changes in the response of trigeminal
359 neurons to neurotrophins: Influence of birthdate and the ganglion environment. *Development*
360 **126**, 4365–4373 (1999).

361 37. Steventon, B., Mayor, R. & Streit, A. Neural crest and placode interaction during the development
362 of the cranial sensory system. *Dev Biol* **389**, 28–38 (2014).

363 38. York, J. R., Yuan, T. & McCauley, D. W. Evolutionary and Developmental Associations of Neural
364 Crest and Placodes in the Vertebrate Head: Insights From Jawless Vertebrates. *Frontiers in*
365 *Physiology* vol. 11 986 Preprint at https://doi.org/10.3389/fphys.2020.00986 (2020).

366 39. Méndez-Maldonado, K., Vega-López, G. A., Aybar, M. J. & Velasco, I. Neurogenesis From Neural
367 Crest Cells: Molecular Mechanisms in the Formation of Cranial Nerves and Ganglia. *Front Cell Dev*
368 *Biol* **8**, (2020).

369 40. Xu, H., Dude, C. M. & Baker, C. V. H. Fine-grained fate maps for the ophthalmic and
370 maxillomandibular trigeminal placodes in the chick embryo. *Dev Biol* **317**, 174–186 (2008).

371 41. Kee, Y., Byung, J. H., Sternberg, P. W. & Bronner-Fraser, M. Evolutionary conservation of cell
372 migration genes: From nematode neurons to vertebrate neural crest. *Genes Dev* **21**, 391–396
373 (2007).

374 42. Yajima, H. *et al.* Six1 is a key regulator of the developmental and evolutionary architecture of
375 sensory neurons in craniates. *BMC Biol* **12**, 1–18 (2014).

376 43. Hamburger, V. & Hamilton, H. L. A series of normal stages in the development of the chick
377 embryo. *Developmental Dynamics* **195**, 231–272 (1992).

378 44. Bolger, A. M., Lohse, M. & Usadel, B. Trimmomatic: A flexible trimmer for Illumina sequence data.
379 *Bioinformatics* **30**, 2114–2120 (2014).

380 45. Andrews, S. FastQC: A quality control tool for high throughput sequence data [Online]. Available
381 online at http://www.bioinformatics.babraham.ac.uk/projects/fastqc/. (2010).

382 46. Kim, D., Langmead, B. & Salzberg, S. L. HISAT: A fast spliced aligner with low memory
383 requirements. *Nat Methods* **12**, 357–360 (2015).

384 47. Anders, S., Pyl, P. T. & Huber, W. HTSeq-A Python framework to work with high-throughput
385 sequencing data. *Bioinformatics* **31**, 166–169 (2015).

386 48. Love, M. I., Huber, W. & Anders, S. Moderated estimation of fold change and dispersion for RNA-
387 seq data with DESeq2. *Genome Biol* **15**, (2014).

388 49. Siersbfk, R. *et al.* Extensive chromatin remodelling and establishment of transcription factor
389 hotspots during early adipogenesis. *EMBO Journal* **30**, 1459–1472 (2011).

390 50. Madsen, J. G. S. *et al.* Highly interconnected enhancer communities control lineage-determining
391 genes in human mesenchymal stem cells. *Nat Genet* **52**, 1227–1238 (2020).

392 51. Wickham, H. ggplot2: Elegant graphics for data analysis. Springer-Verlag New York. ISBN 978-3-
393 319-24277-4, https://ggplot2.tidyverse.org. (2016).

394 52. Nasir, A. *et al.* The integration of Tgfβ and Egfr signaling programs confers the ability to lead
395 heterogeneous collective invasion. *bioRxiv* 2020.11.14.383232 (2023)
396 doi:10.1101/2020.11.14.383232.

397 53. Xie, Z. *et al.* Gene Set Knowledge Discovery with Enrichr. *Curr Protoc* **1**, (2021).

398 54. Chen, E. Y. *et al. Enrichr: Interactive and Collaborative HTML5 Gene List Enrichment Analysis Tool*.
399 http://amp.pharm.mssm.edu/Enrichr. (2013).

400 55. Kuleshov, M. V. *et al.* Enrichr: a comprehensive gene set enrichment analysis web server 2016
401 update. *Nucleic Acids Res* **44**, W90–W97 (2016).

402 56. Aleksander, S. A. *et al.* The Gene Ontology knowledgebase in 2023. *Genetics* **224**, (2023).

403 57. Allen, E. A. & Baehrecke, E. H. Autophagy in animal development. *Cell Death and Differentiation*
404 vol. 27 903–918 Preprint at https://doi.org/10.1038/s41418-020-0497-0 (2020).

405 58. Valencia, M., Kim, S. R., Jang, Y. & Lee, S. H. Neuronal autophagy: Characteristic features and roles
406 in neuronal pathophysiology. *Biomolecules and Therapeutics* vol. 29 605–614 Preprint at
407 https://doi.org/10.4062/BIOMOLTHER.2021.012 (2021).

408 59. Deng, Z., Zhou, X., Lu, J. H. & Yue, Z. Autophagy deficiency in neurodevelopmental disorders. *Cell*
409 *and Bioscience* vol. 11 Preprint at https://doi.org/10.1186/s13578-021-00726-x (2021).

410 60. Putra, V. D. L., Kilian, K. A. & Knothe Tate, M. L. Biomechanical, biophysical and biochemical
411 modulators of cytoskeletal remodelling and emergent stem cell lineage commitment.
412 *Communications Biology* vol. 6 Preprint at https://doi.org/10.1038/s42003-022-04320-w (2023).

413 61. Shellard, A. & Mayor, R. Integrating chemical and mechanical signals in neural crest cell migration.
414 *Curr Opin Genet Dev* **57**, 16–24 (2019).

415 62. Roycroft, A. *et al.* Redistribution of Adhesive Forces through Src/FAK Drives Contact Inhibition of
416 Locomotion in Neural Crest. *Dev Cell* **45**, 565-579.e3 (2018).

63. Smith, G. M. & Gallo, G. The role of mitochondria in axon development and regeneration. *Developmental Neurobiology* vol. 78 221–237 Preprint at https://doi.org/10.1002/dneu.22546 (2018).

64. Vaarmann, A. *et al.* Mitochondrial biogenesis is required for axonal growth. *Development (Cambridge)* **143**, 1981–1992 (2016).

65. Patthey, C. *et al.* Identification of molecular signatures specific for distinct cranial sensory ganglia in the developing chick. *Neural Dev* **11**, 1–20 (2016).

Figures and Legends

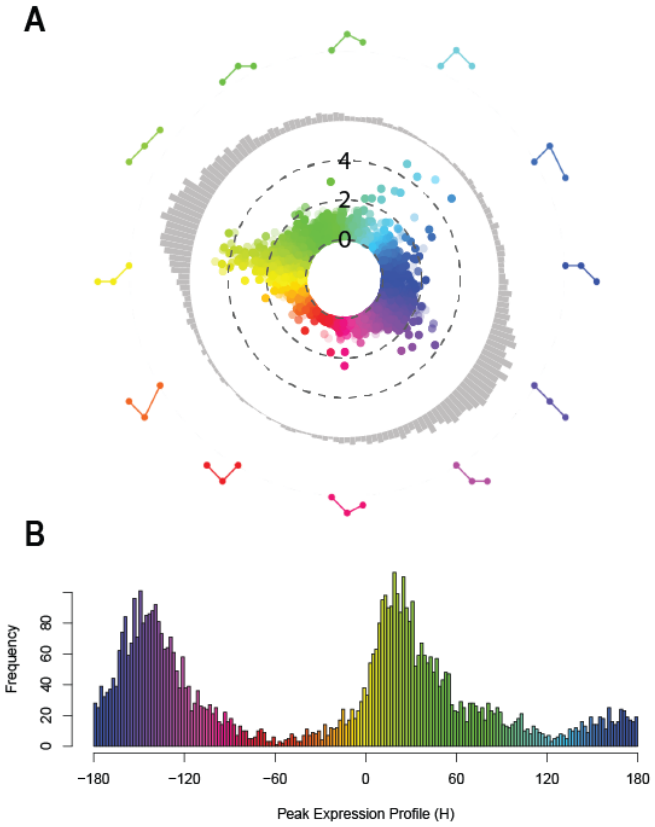

Figure 1. Temporally dynamic relative transcript expression during chick trigeminal ganglion development. A) Polar plot depicting relative temporal relationships of differentially expressed genes detected in the HH13/14, HH15/16, and HH17/18 chick trigeminal ganglion. Individual genes are represented as single points based on changes in expression across the three timepoints. In the three-point angular profiles surrounding the circular plot, the left dot represents HH13/14, the middle dot represents HH15/16, and the right dot represents HH17/18, whereas the pattern of each profile demonstrates the relative relationship of a gene's expression at a given degree along the circular plot, i.e. the yellow profile represents a gene that does not change from HH13/14 to HH15/16, but is significantly upregulated from HH15/16 to HH17/18. Genes exhibiting a maximum Log_2 fold change deemed significant ($p<0.05$ after Benjamini-Hochberg correction) at one timepoint relative to at least one other (three total comparisons) are shown. Maximal Log_2 fold change for each gene is represented as distance from the center, while the concentric dotted lines represent Log_2 fold change thresholds of 0, 2, and 4, respectively, from the center of the plot moving outward. Gray bars around the outer circumference demonstrate the number of genes at any given degree along the circle, which are transformed to a straight axis in B. **B)** Color-coded histogram illustrating the number of genes at any given degree ("H") along the circumference of the polar plot, where 0 degrees equates to the yellow three-point profile in A.

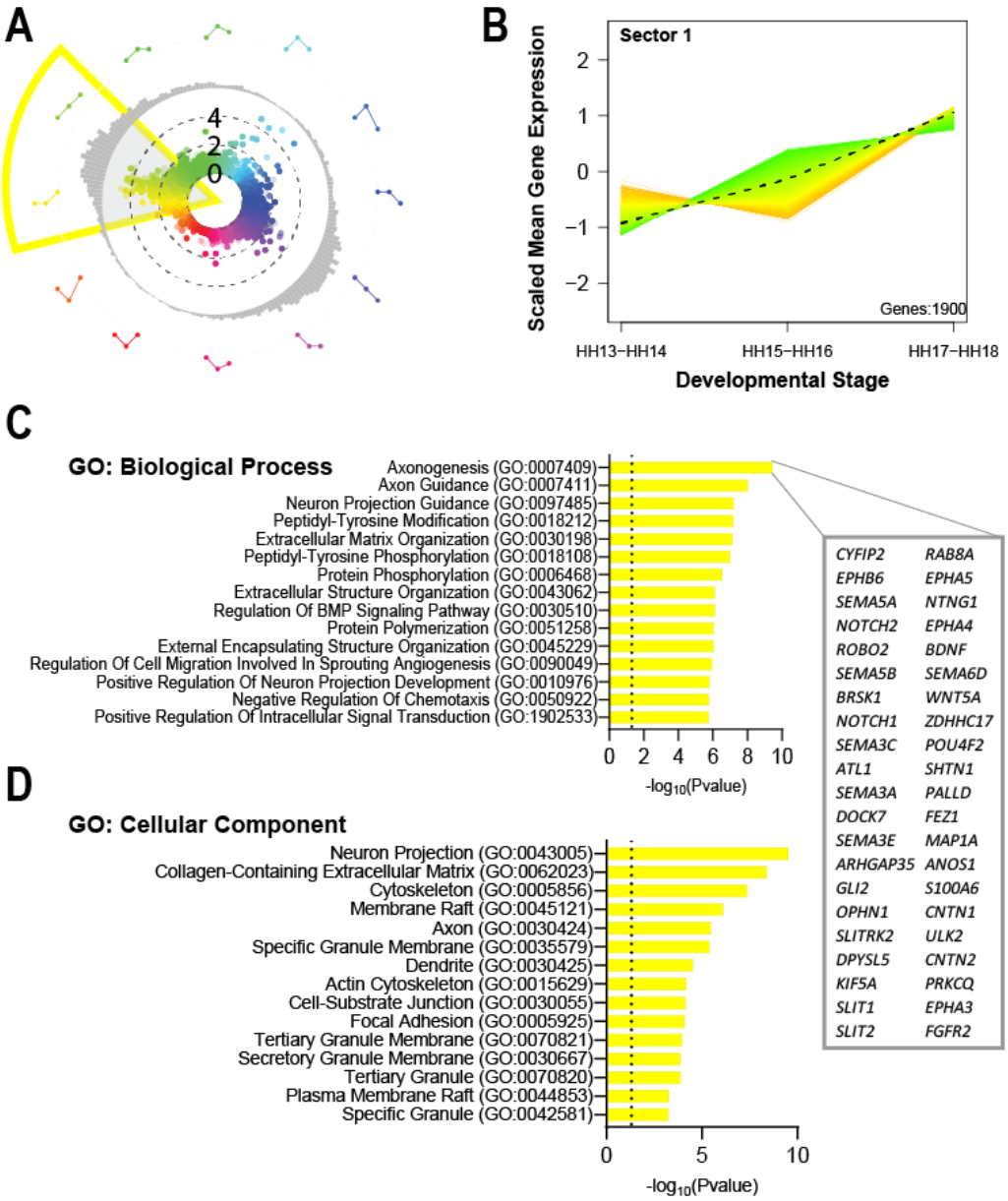

Figure 2. Genes associated with neuron development and axon guidance are continuously upregulated between HH13/14 and HH17/18 in the chick trigeminal ganglion. A) The yellow wedge overlayed on the polar plot represents the 60-degree angle used to define Sector 1 for gene ontology enrichment. **B)** Color-coded line plots reveal the relative expression patterns of individual genes included in Sector 1. The dotted line is the average scaled gene expression of all genes in Sector 1. **C-D)** Bar graphs illustrate the fifteen most enriched biological processes (C) and cellular components (D) associated with Sector 1 genes (Fisher's exact test), in order of transformed p-value. The box outlined to the right lists all genes from Sector 1 associated with Axonogenesis (GO:0007409).

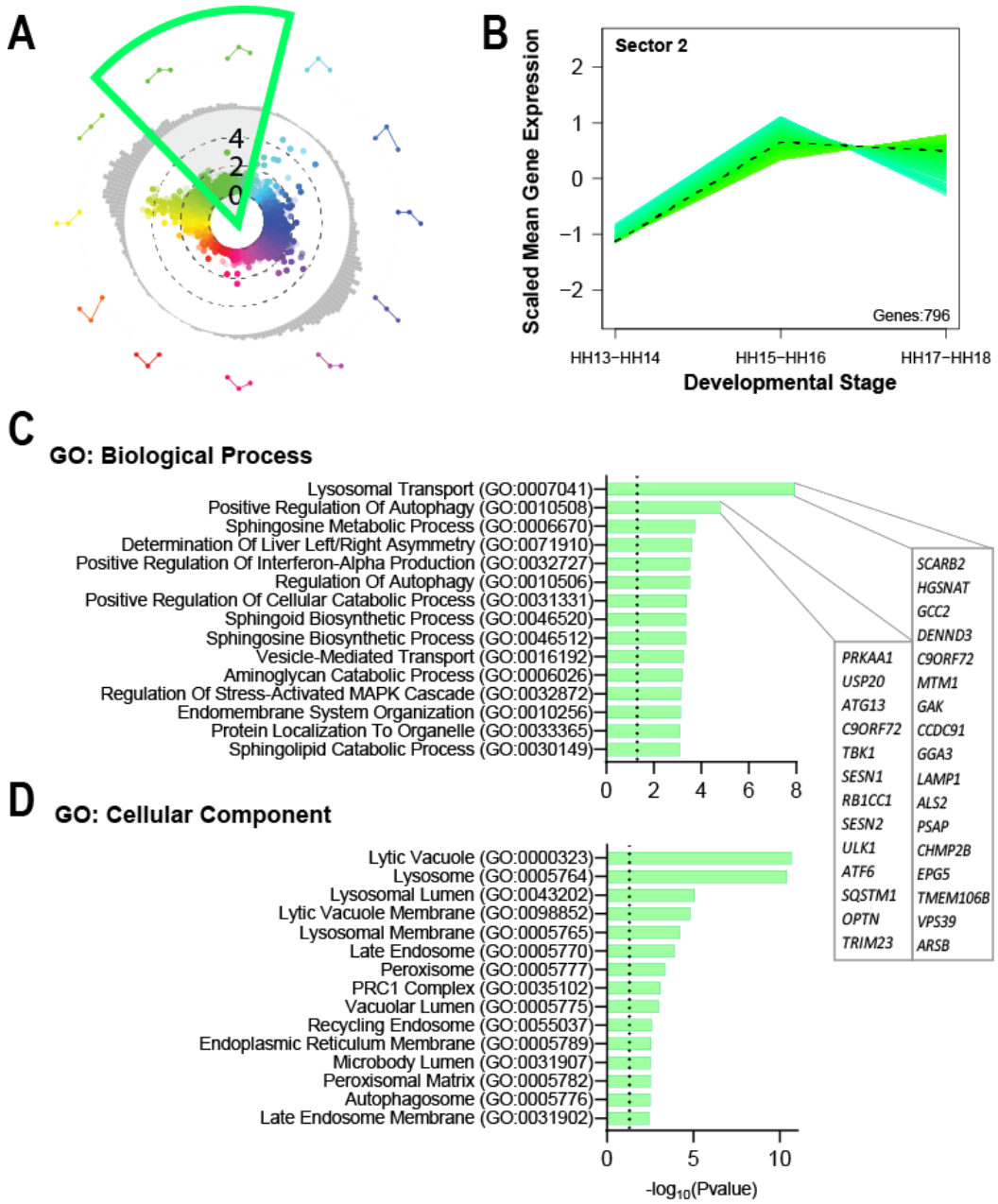

Figure 3. Autophagy-related genes are upregulated from HH13/14 to HH15/16, and maintained at HH17/18, in the chick trigeminal ganglion. A) The green wedge overlayed on the polar plot represents the 60-degree angle used to define Sector 2 for gene ontology enrichment. **B)** Color-coded line plots reveal the relative expression patterns of individual genes included in Sector 2. The dotted line is the average scaled gene expression of all genes in Sector 2. **C-D)** Bar graphs illustrate the fifteen most enriched biological processes (C) and cellular components (D) associated with Sector 2 genes (Fisher's exact test), organized by transformed p-value. The box outlined to the right lists all genes from Sector 2 associated with Lysosomal Transport (GO:0007041) and Positive Regulation of Autophagy (GO:0010508).

Supplemental Figures and Legends

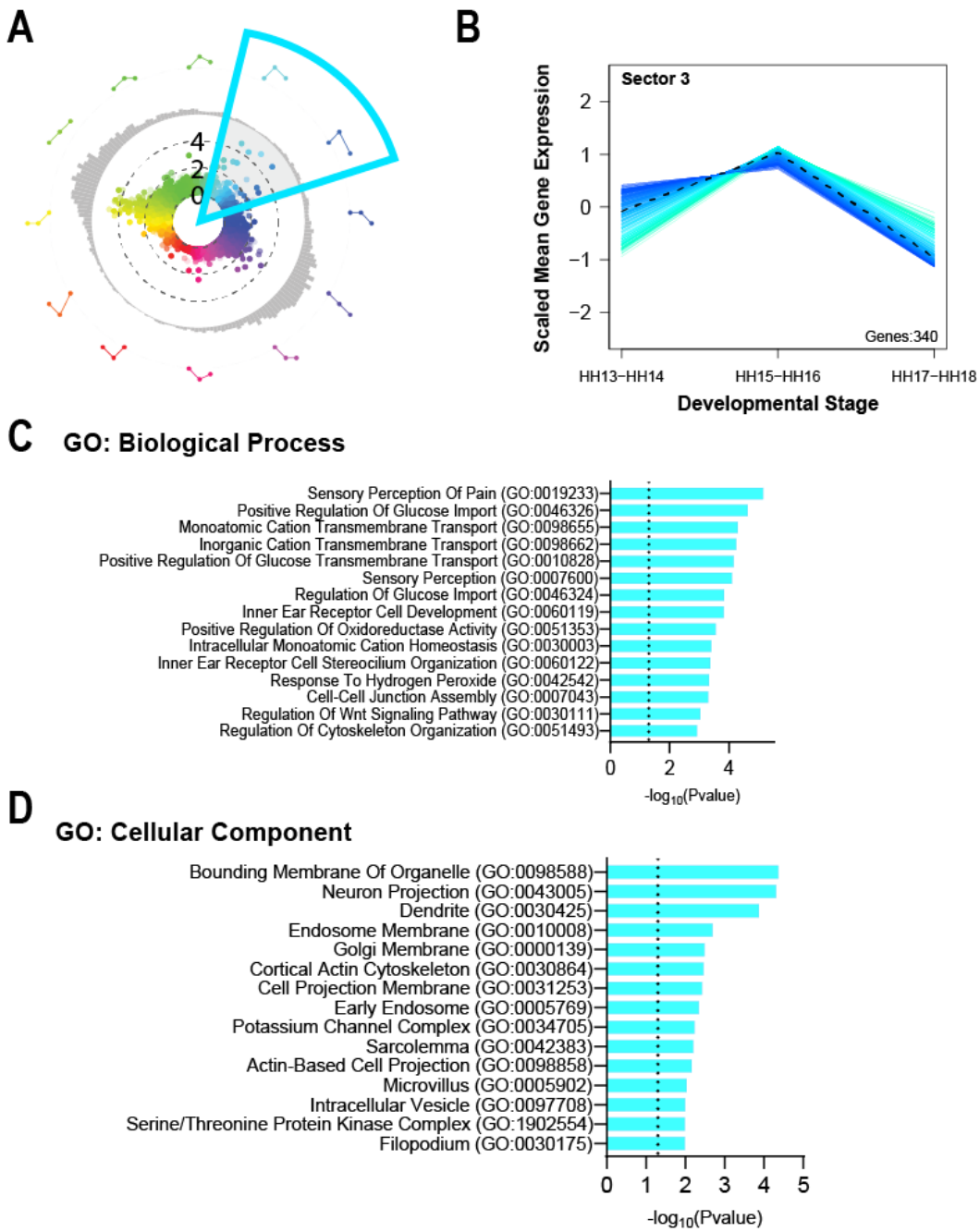

Supplemental Figure 1. Sector 3 gene expression and ontologies. A) The light blue wedge overlayed on the polar plot from Figure 1 represents the 60-degree angle used to define Sector 3 for gene ontology enrichment. **B)** Color-coded line plots reveal the relative expression patterns of individual genes included in Sector 3. The dotted line is the average scaled gene expression of all genes in Sector 3. **C-D)** Bar graphs illustrate the fifteen most enriched biological processes (C) and cellular components (D) associated with Sector 3 genes (Fisher's exact test), organized by transformed p-value.

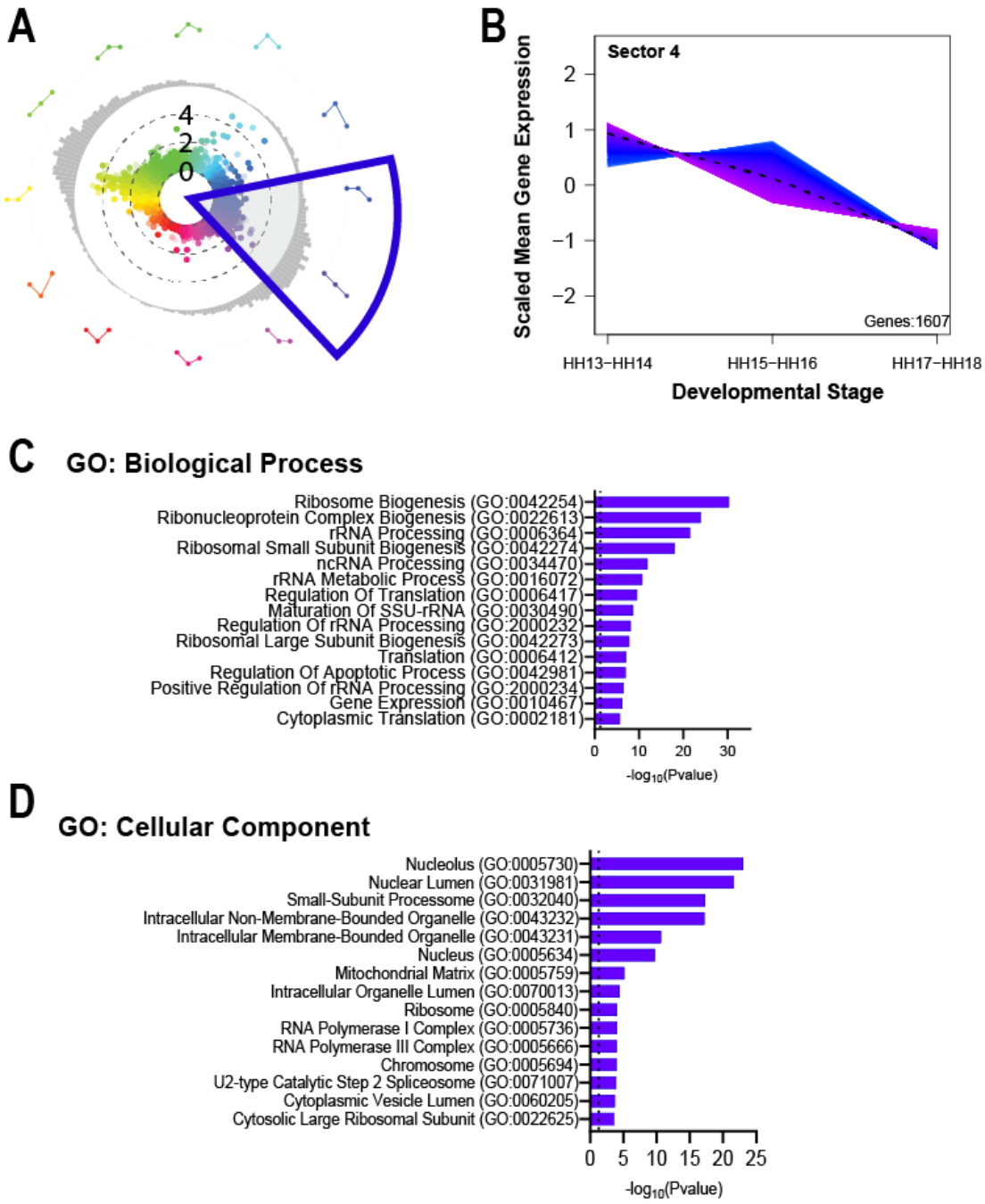

Supplemental Figure 2. Sector 4 gene expression and ontologies. A) The dark blue wedge overlayed on the polar plot from Figure 1 represents the 60-degree angle used to define Sector 4 for gene ontology enrichment. **B)** Color-coded line plots reveal the relative expression patterns of individual genes included in Sector 4. The dotted line is the average scaled gene expression of all genes in Sector 4. **C-D)** Bar graphs illustrate the fifteen most enriched biological processes (C) and cellular components (D) associated with Sector 4 genes (Fisher's exact test), organized by transformed p-value.

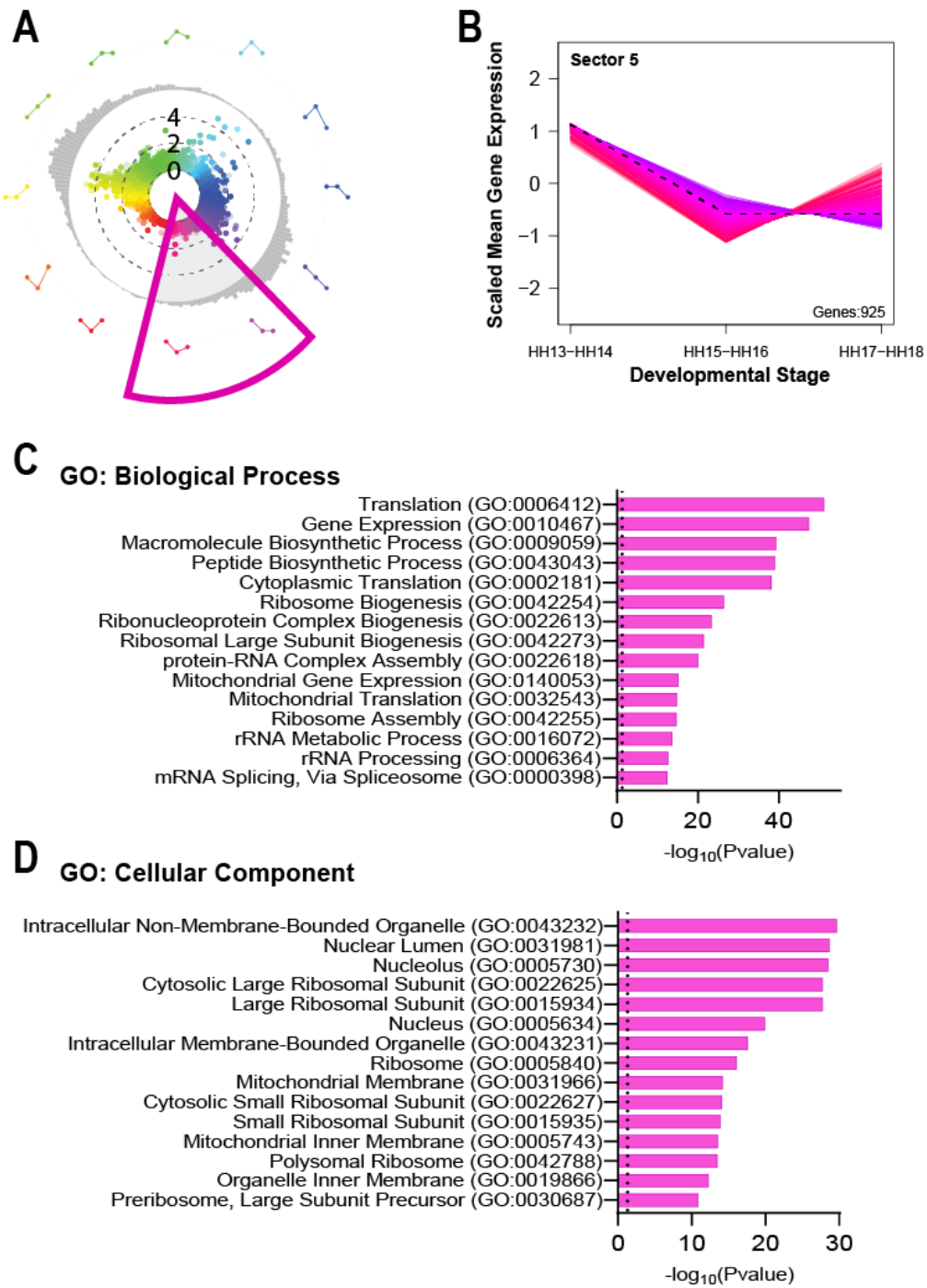

Supplemental Figure 3. Sector 5 gene expression and ontologies. A) The pink wedge overlayed on the polar plot from Figure 1 represents the 60-degree angle used to define Sector 5 for gene ontology enrichment. **B)** Color-coded line plots reveal the relative expression patterns of individual genes included in Sector 5. The dotted line is the average scaled gene expression of all genes in Sector 5. **C-D)** Bar graphs illustrate the fifteen most enriched biological processes (C) and cellular components (D) associated with Sector 5 genes (Fisher's exact test), organized by transformed p-value.

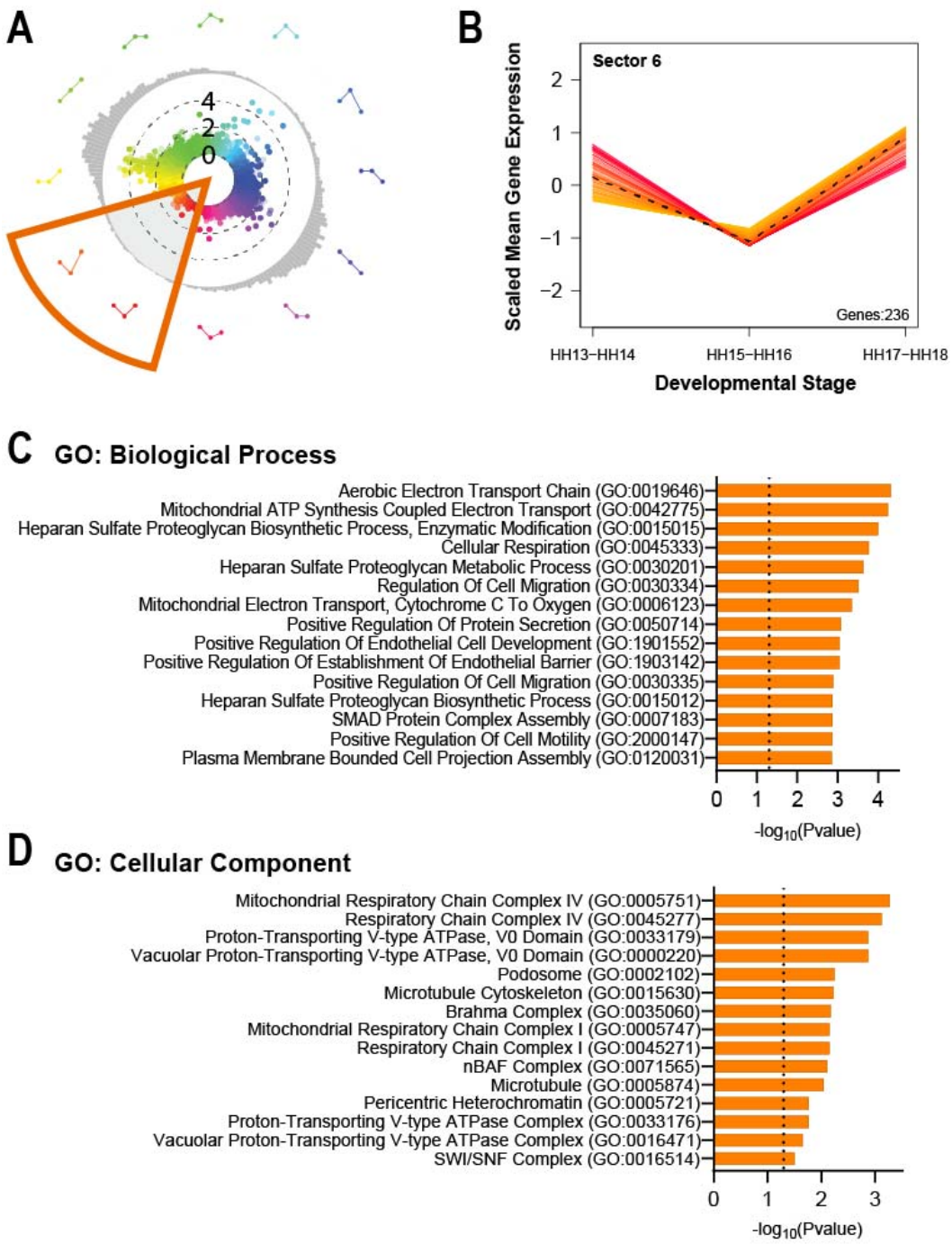

Supplemental Figure 4. Sector 6 gene expression and ontologies. A) The orange wedge overlayed on the polar plot from Figure 1 represents the 60-degree angle used to define Sector 6 for gene ontology enrichment. **B)** Color-coded line plots reveal the relative expression patterns of individual genes included in Sector 6. The dotted line is the average scaled gene expression of all genes in Sector 6. **C-D)** Bar graphs illustrate the fifteen most enriched biological processes (C) and cellular components (D) associated with Sector 6 genes (Fisher's exact test), organized by transformed p-value.

Supplemental Data Files

Supplemental File 1. Color-coded Excel spreadsheet containing calculated values for differential expression comparisons and polar plot.

Supplemental File 2. Excel spreadsheets compiling gene ontology enrichment results for Biological Processes (BP) and Cellular Components (CC) associated with each 60-degree polar plot sector.

Supplemental File 3. Tab-delimited text file with normalized gene counts from each timepoint examined in chick trigeminal ganglion.

Supplemental File 4. Tab-delimited text file with normalized gene counts of genes differentially expressed in chick trigeminal ganglion between HH13/14 and HH15/16.

Supplemental File 5. Tab-delimited text file with normalized gene counts of genes differentially expressed in chick trigeminal ganglion between HH15/16 and HH17/18.

Supplemental File 6. Tab-delimited text file with normalized gene counts of genes differentially expressed in chick trigeminal ganglion between HH13/14 and HH17/18.